Research article

Lattice variation as a function of concentration and grain size in MgO–NiO solid solution system

Chen Barad [a], Giora Kimmel [b,*], Agnieszka Opalińska [c], Stanislaw Gierlotka [c], Witold Łojkowski [c]

[a] NRCN, P.O. Box 9001, Beer-Sheva, 84190, Israel
[b] Department of Materials Engineering, Ben-Gurion University of the Negev, Beer-Sheva, 84105, Israel
[c] Institute of High Pressure Physics, Polish Academic of Sciences (PAS), Warszawa, Poland

A B S T R A C T

The study aimed to understand how changes in crystal's size affect the lattice parameters and crystal structure of $Mg_{1-x}Ni_xO$ solid solution for six X values ranging from x = 0 to x = 1. $Mg_{1-x}Ni_xO$ was synthesized via two different wet-chemical techniques: the sol-gel and the microwave hydrothermal method, both followed by calcination at different temperatures of 673, 873, 1073, 1273 and 1473 K. As annealing caused grain growth, the varied temperature range allowed to examine a wide range of grain sizes. The lattice parameters and x values were determined from XRD (X-ray diffraction) peak positions and intensities respectively. The grain size was evaluated by XRD line profile analysis and supported by SEM (scanning electron microscope) observations. At the temperatures of 673 and 873 K grain size was in the nanometric range and from 1073 K and above grain size was in the micrometric range. A non-monotonic lattice variation versus grain size was found for each concentration. When grain size decreased there was a slight contraction, however for grain size in the nanometric range there was a severe lattice expansion. Both lattice parameter changes were explained by two effects acting together: contraction due to surface stress and expansion due to weakening of the ionic bonding at nanocrystalline particles. In this current research study, the lattice parameter was mapped in two dimensions: concentration and grain size. The findings of this study provided valuable insights into the lattice variation in the MgO–NiO solid solution system.

1. Introduction

Nickel oxide (NiO) and magnesium oxide (MgO) are of great importance in a variety of applications and in diverse fields both as individual ceramic oxide materials and as a binary system of $Mg_{1-x}Ni_xO$ with x ranging from 0 to 1. Both MgO and NiO are ionic compounds with different crystal structures, and their lattice parameters can vary depending on composition and phase transformations.

NiO is a significant transition metal oxide with a cubic lattice structure known as the rock-salt structure with a slight distortion. It is a face-centered cubic FCC arrangement of oxide ions (O^{2-}), but nickel ions (Ni^{2+}) occupy both the octahedral and the tetrahedral sites. The lattice parameter of pure NiO at room temperature is 4.175 Å. Nano particles of nickel oxide (NiO) play a major role in myriad

* Corresponding author.
  E-mail address: giorakimmel@gmail.com (G. Kimmel).

fields such as in: molecular biology and biotechnology [1], catalysis [2], battery cathodes [3,4], gas sensors [5], electrochromic films [6] and magnetic materials [7,8]. In addition, NiO_x is also used in reactions of hydrogenation of nitriles and the hydrochlorination of aromatic compounds [9,10]. Moreover, NiO films with Mn and Zn doping have been fabricated successfully using a homemade chemical spray pyrolysis thin films deposition technique producing transparent conducting oxides emerging applicability of the films in optoelectronic applications [11].

MgO has also a rock-salt crystal structure, which is an FCC arrangement of oxide ions (O^{2-}) with magnesium ions (Mg^{2+}) occupying the octahedral sites between them. The lattice parameter of pure MgO at room temperature is approximately 4.213 Å. MgO nanoparticles have been recently used in various domains due to their simple synthesis methods (such as the sol-gel and co-precipitation techniques) [12,13] along with their exceptional properties (such as biodegradability and biocompatibility) [14]. Among their many uses, the main applications include: biological implants (due to their high strength to weight ratio, low density and etc.), in biomedical for bone regeneration as a medicine for anti-bactericidal and antimicrobial inhibition and in cryoinjury applications [15–18] and in cancer therapy [19]. They are also employed in sorption of uranium ions [20], catalysis [21,22] and lithium-ion batteries [23,24]. MgO is also applicable in environmental uses such as water purification [25] and in synthetic dyes promoting degradation of harmful dyes [26], photonics applications [27] and the purified form of magnesium oxide nano powder is used to improve mechanical and fabrication characteristics of aluminium as an alloy [28,29]. In civil engineering, MgO is effective in preventing the thermal cracking of mass concretes, such as dams and diversion tunnels owing to the thermal shrinkage compensating property of MgO [30].

The joint system of NiO with MgO offers several interesting properties and potential applications due to the unique characteristics of each material. MgO is known for its excellent thermal and chemical stability, while NiO has good structural stability. Combining these materials can lead to enhanced stability, making the joint system suitable for applications in harsh environments or high-temperature conditions. In addition, NiO and MgO have similar crystal structures, with both adopting the rock salt (NaCl) structure. This lattice compatibility enables the formation of high-quality interfaces and heterostructures between the two materials, with minimal lattice mismatch. This can result in improved electronic, optical, and transport properties at the interface. The joint system of NiO–MgO has also been extensively studied for its catalytic properties. NiO exhibits catalytic activity for various reactions, such as CO oxidation and hydrocarbon reforming, while MgO is known for its basicity and ability to promote reactions involving acid-base interactions. Combining these materials can create synergistic effects, leading to enhanced catalytic performance and selectivity [31,32]. Furthermore, NiO is an antiferromagnetic material with a Néel temperature above room temperature. By integrating NiO with MgO, which is a good insulator with excellent electrical properties, it is possible to create spintronic devices that utilize the antiferromagnetic properties of NiO. The exchange coupling at the NiO/MgO interface can be exploited for spin injection, manipulation, and detection, making it promising for spin-based electronics. Optoelectronics and energy conversion technologies are other applications of the NiO–MgO system. For example, NiO is a p-type semiconductor, while MgO is an insulator with a wide bandgap. By forming heterostructures or composite materials, the joint system can exhibit unique optical and electrical properties suitable for solar cells, sensors, and other energy conversion devices [33–36].

This system was also researched regarding the preparation conditions aiming to control the morphology and particle size of the NiO phase [37].

The binary phase diagram of the MgO–NiO system displays a solid solution over the full range of relative concentration. The lattice parameter of a solid solution in a binary system depends on the relative concentrations of the components. The Vegard's law is often used as an approximation to estimate the lattice parameter of an ideal binary solid solution:

$$a = x \bullet a_{MgO} + (1 - x) \bullet a_{NiO} \tag{1}$$

where "a" is the lattice parameter of the mixed system, "x" is the mole fraction of MgO, "a_{MgO}" is the lattice parameter of MgO, and "a_{NiO}" is the lattice parameter of NiO. So, as the concentration of MgO increases in the MgO–NiO system, the lattice parameter will tend to approach the lattice parameter of pure MgO, and vice versa.

In ionic crystals where alternating cations and anions held together by electrostatic forces one of the most important physical dimensions is the lattice parameter. The lattice parameter is a fundamental property affecting the functional properties of the material. Anomalously, the lattice constant in nano-crystals is not a constant [38]. The lattice parameter, along grain size shows a non-monotonic trend, namely a decrease in the lattice parameter when crystal size increases (or alternatively, lattice expansion for decreasing crystal size) to a minimum value and then the lattice parameter increases with size up to a constant value for larger grain size [39]. For example, a lattice contraction of nanocrystalline anatase (TiO_2) as a function of particle size (4–34 nm) was shown revealing an unexpected strong size dependence [40]. General equations derived from theoretical calculations describing lattice contraction and surface stress in nanocrystals were also established explaining this behavior [41]. A non-monotonic lattice variation as a function of grain size in nanocrystalline CeO_2 was also reported showing a minimum value of lattice parameter in grain size between 25 and 50 nm [42]. Those findings showed that this anomalous dependence of the lattice parameter on crystal size was not exclusive for metals as though. The size effect in metals was well investigated [43,44], modeled [45,46] and especially studied regarding their electrical conductivity [47–49] and the influence of size on the elastic constants (Young's modulus and Poisson's ratio) in thin tungsten films [50], but also mentioned in ceramics concerning conductivity in SnO_2 [51] and in barium titanate glass-ceramic [52].

One of the most likely to be affected by the grain size is the catalytic activity [53]. Other properties that might be affected by the grain size are: mechanical [54], magnetic, electronic and optical [55–57]. The non-monotonic lattice variation can be explained by two effects acting simultaneously as a function of crystal size: lattice contraction due to capillary forces caused by the surface stress and by a Madelung model predicting lattice expansion due to weakening of bonding force in small ionic crystals [39,58]. In nano ionic crystals, the non-monotonic trend of the lattice parameter as a function of grain size is thought-provoking and important to comprehend.
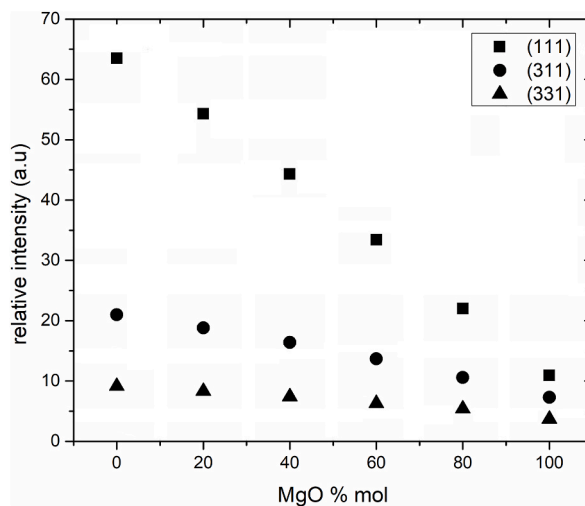
Fig. 1. Relative intensities as a function of composition in the $Mg_{1-x}Ni_xO$ system.
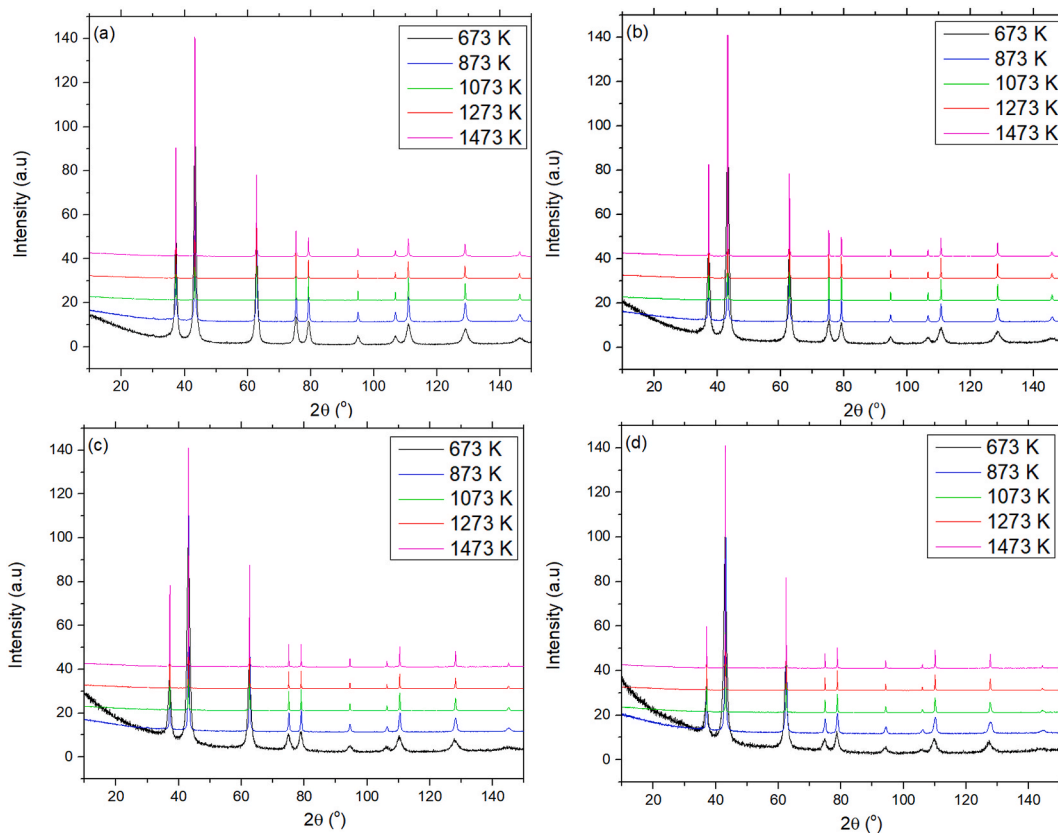
Fig. 2. X-Ray diffraction of the $Mg_xNi_{1-x}O$ system calcined at different temperatures: (a) 20 % MgO, (b) 40 % MgO, (c) 60 % MgO and (c) 80 % MgO.

Studying the influence of grain size along with other well studied parameters of temperature and composition is vital and particularly relevant due to recent applications of nano oxide materials (rather than bulk) in industrial and other nowadays uses [14,59,60]. Exploiting the variation of physical, chemical, and biological properties on grain size is one of the fundaments of nanotechnology.

Among other parameters, powder morphology has a crucial part in ensuring the consistency and reproducibility in production processes (such as in thermal spraying [61] and in sintering). In addition, powder morphology has a role in determining functionality
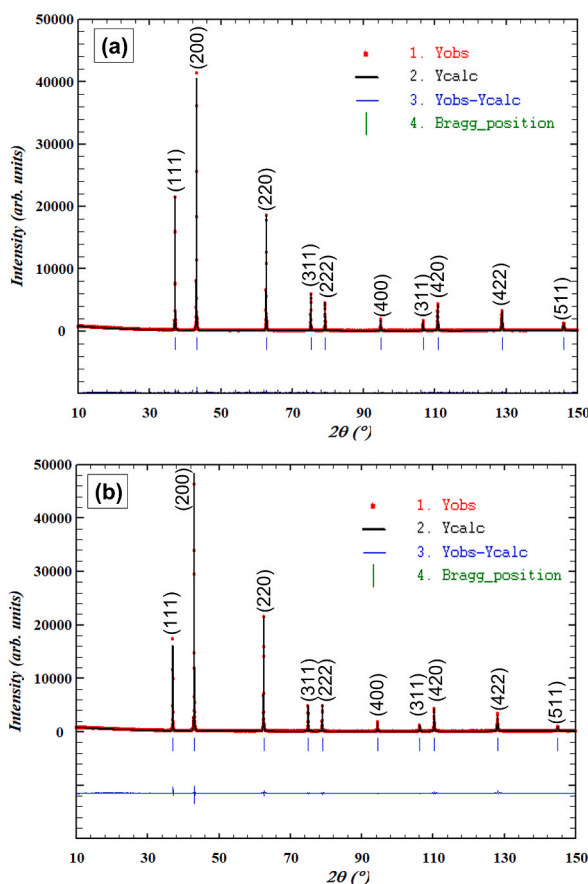
Fig. 3. Rietveld refinement of: (a) 20 % MgO calcined at 800 °C and (b) 60 % MgO calcined at 1200 °C.

in applications such as dry-powder inhalers (controlling and optimizing drugs delivery) [62] and in catalysis processes [63,64]. Therefore, an exploration of not only size but also shape is of great interest.

Although some studies investigating the crystallographic properties of the NiO–MgO system exist, a profound analysis regarding the lattice parameter behaviour as a function of grain size is lacking [65,66]. Lattice variations in the nano system of NiO–MgO can have significant implications for the material's properties and performance. The lattice parameter variations can further influence the band structure, bandgap, and electronic properties of the composite, potentially leading to changes in its optical, electrical, and magnetic behaviour [67–69].

In summary, lattice variations in the nano system of NiO–MgO have a profound impact on the material's structure, electronic properties, catalytic activity, size-dependent phenomena, and interface behaviour. Understanding and controlling these lattice variations are crucial for tailoring the properties of NiO–MgO nanostructures for diverse applications. Therefore, the current study aims to better comprehend the influence of parameters such as concentration, temperature and also grain size on the structural properties yielding a better understanding of the lattice variations in the nano system of NiO–MgO.

2. Material and methods

The $Mg_{1-x}Ni_xO$ powder was synthesized using the microwave solvothermal method. Firstly, nickel (II) acetate and magnesium (II) acetate were dissolved in water. The ratio of nickel acetate to magnesium acetate was adjusted to obtain the desired range of the different compositions of the $Mg_{1-x}Ni_xO$ particles (compositions of: 0, 20, 40, 60, 80, 100 mol % MgO). The joined concentration of both acetates was 0.5 M. The solution was neutralized with NaOH to pH of 10. Then the solution was poured into a Teflon vessel that was tightly closed and inserted into the Ertec microwave reactor (ERTEC-Poland). Subsequently the 250 W microwave power was switched on and the content was heated for 30 min at pressure of 6 MPa which corresponds to 230 °C. After cooling down, the product was poured on a paper filter and washed 3 times with distiller water. Afterwards, the product was dried in air for 24 h. Lastly, the samples were calcined in an electric furnace starting from room temperature to the desired final temperature (varied from 400° to 1200 °C) for 30 min.

X-ray diffraction (XRD) measurements were performed using an X'Pert PRO diffractometer (Panalytical, Almelo, The Netherlands). The XRD diffractions were collected at room temperature in the range of 2θ between 10 and 100 °2θ° and with a step of 0.03 °2θ. Some
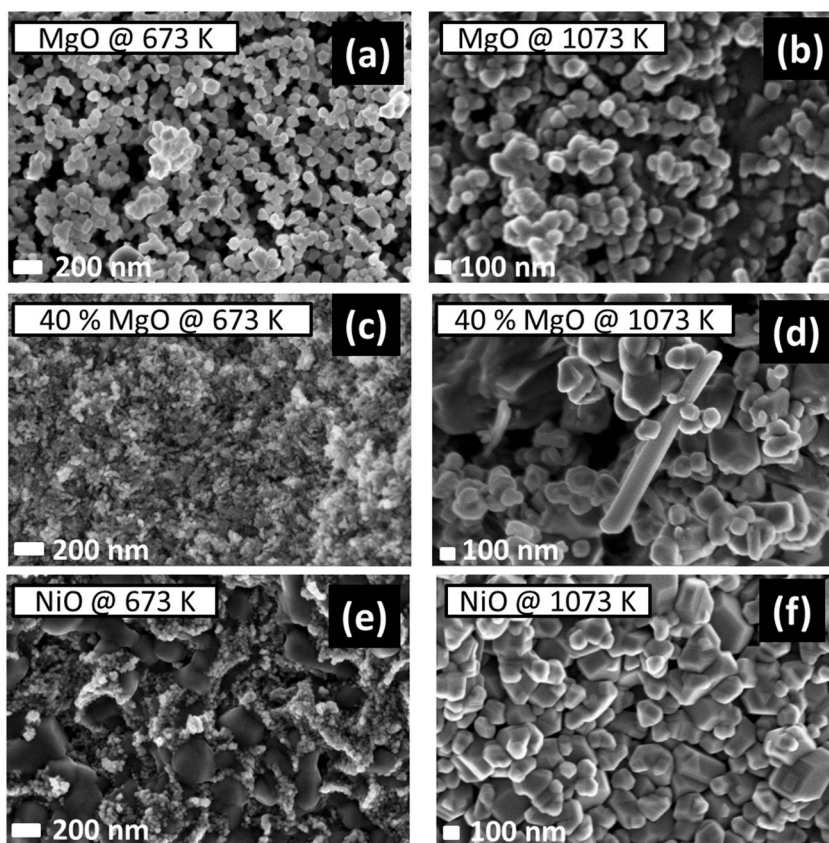
Fig. 4. SEM images (magnitude of 100,000×) of $Mg_{1-x}Ni_xO$ systems calcined at different calcination temperatures.

powder samples were run in transmission mode on a diffractometer consisted of a Huber Guinier digitized camera equipped with a Fuji imaging plate detector and a rotating Cu anode, operated in 45 KV and 80 mA. The scanning range was from 4 to 100°2θ. The data were read by a laser beam with a light detector, in steps of 0.005°2θ scale and the exposure time was 10 min. In both systems an incident beam monochromator provided pure Cu $K\alpha_1$ source.

SRM 660b (LaB_6) was used for line position and instrumental width standards. Rietveld method [70] was applied using the public domain program [71] for refinement of the lattice parameters, site occupancies and providing information about the peaks' profiles. Program and Rietveld refinement was also carried out using the FullProf/WinPLOTR software [72]. Powder-Cell for Windows [73] was used for strain and size analysis evaluation based on the Williamson-Hall method. The line profile parameters were inserted from data obtained by the FullProf analysis. Since the line broadening is sensitive to the background subtraction, we calculated the grain size (GS) and microstrain (MS) by using both approximation for background subtraction. β = B-b and β = B-b²-, where β is the determined peak broadening, B the global experimental peak width and b the instrumental width. GS from electron microscopy observations was also used to verify the XRD's GS results. This procedure for obtaining accurate GS and MS values was carefully examined and reported in a previous publication [42].

In addition to the samples produced via the microwave solvothermal method, a different set of pure NiO and MgO samples were synthesized by the conventional sol-gel technique. The hydroxide $Ni(OH)_2$ or $Mg(OH)_2$ was precipitated from water solution of $NiCl_2$ or $MgCl_2$ by raising the PH value by adding NH_4OH or NaOH. After separation of the solid hydroxide from the liquid solution and drying in air for a week, the hydroxide xerogel was obtained. The obtained powder was formed by firing the xerogel at different desired temperatures from 200 up to 1200 °C for 3 h by inserting the samples directly into a hot furnace at the desired final calcination temperature.

The composition of each sample was refined based on the XRD analysis (Rietveld method). The Rietveld structural analysis was conceivable and sensitive to the changes in intensities in the $Mg_{1-x}Ni_xO$ system due to a significant difference in intensities as a function of concentration (as shown in Fig. 1). Since the lattice parameters are only reflected in the Bragg peak positions and determined independently of intensities, they were used to confirm the compositions obtained based on the intensity analysis via checking if the results comply with Vegard's law.

The morphology of the samples was investigated using a scanning electron microscope (SEM) ULTRA PLUS (ZEISS, Oberkochen, Germany) and the average grain size was estimated by analysing the well-defined grains using *imageJ* software (image processing software). Before performing the SEM observations, the samples were coated with a thin carbon layer in order to prevent charging
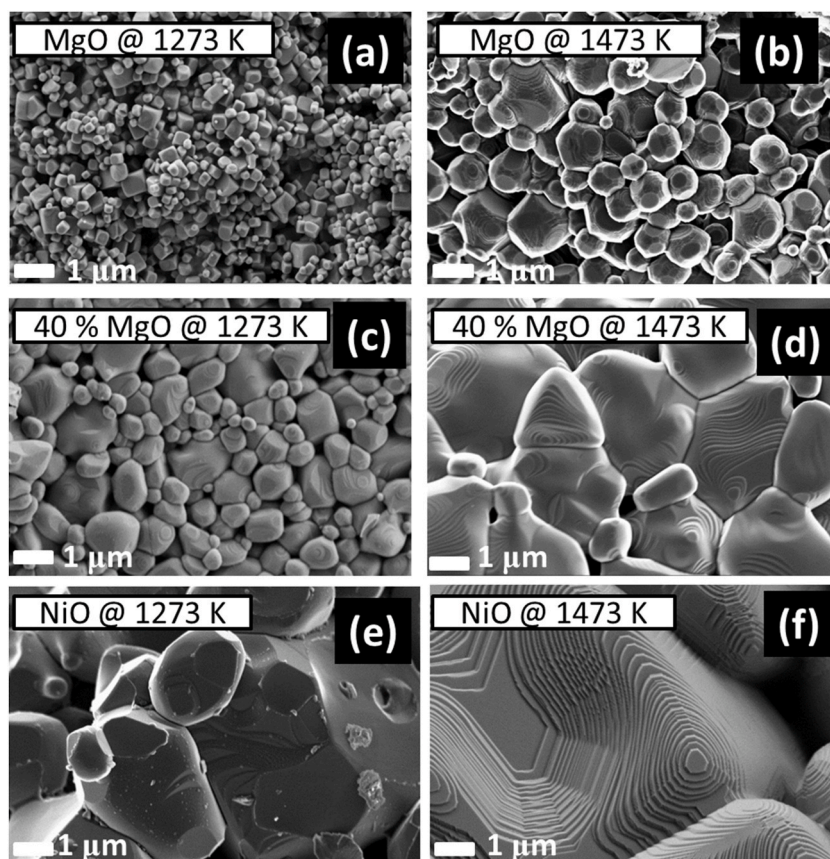
Fig. 5. SEM images (magnitude of 25,000×) of $Mg_{1-x}Ni_xO$ systems calcined at different calcination temperatures.

mechanisms that cause material surface deterioration.

3. Results and discussion

3.1. X-Ray diffraction analysis and morphology

Fig. 2 shows powder diffraction patterns of the investigated samples. The crystal structure characterization was based on the relative integral intensities and peak positions. The microstructure: grain size and micro-strain was evaluated based on the peaks' widths and shape. In the $Mg_xNi_{1-x}O$ system there were four refined variables: lattice parameter (obtained from the peaks' positions), Mg:Ni ratio (obtained from the relative integral intensities), grain size and micro-strain obtained from the peaks' widths. In all samples, as temperature increased the peaks became sharper due to grain growth with elevated temperatures.

Some representative examples of Rietveld refinements are given Fig. 3.

The morphology and grain size were studied using SEM and some representative SEM images are shown in Figs. 4 and 5.

Fig. 4 illustrates grain coarsening and increased faceting after annealing at 1073 K. Fig. 5 illustrates further grain coarsening and increased faceting after annealing at 1273 K and 1473 K.

3.2. Unit cell parameter as a function of temperature

According to Fig. 6, the lattice parameter was a function of calcination temperature for all samples.

3.3. Composition analysis

The composition of each sample was refined based on the XRD analysis (Rietveld method).

According to Table 1, a systematic shift towards a higher Mg content comparing to the nominal concentrations was apparent in all samples. This shift is explained due to a partial precipitation during the synthesis process. The accurate composition was refined based on the XRD analysis (Rietveld method) as shown in Table 1. Nominal compositions of: 0, 20, 40, 60, 80, 100 mol % MgO were corrected to 0, 22, 44, 71, 83, 100 mol %.
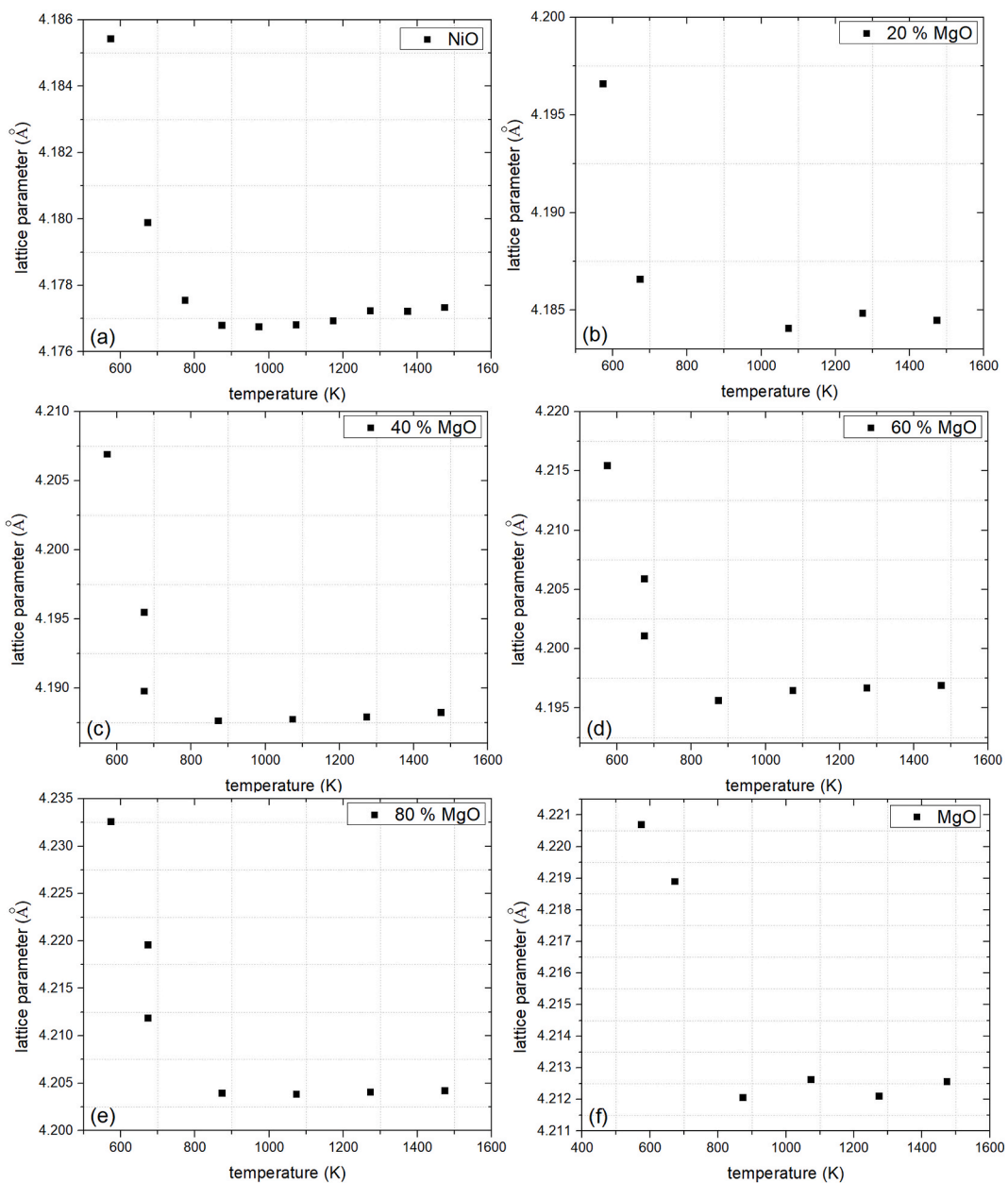
Fig. 6. Unit cell parameter versus calcination temperature for the $Mg_{1-x}Ni_xO$ samples.

Table 1
Refined concentration of NiO in MgO based on XRD analysis using Rietveld method.

	Temperature (K)					Average Mg concentration (%)
	673	873	1073	1273	1473	
Refined concentrations according to Rietveld analysis (%)	0	0	0	0	0	**0**
	21.2	23.8	22.5	22.1	22.4	**22 ± 0.8**
	40.9	42.6	44.5	46.8	46.2	**44 ± 2**
	67.1	71.2	71.1	74.0	73.7	**71 ± 2**
	81.6	82.1	82	83.2	84.9	**83 ± 1**
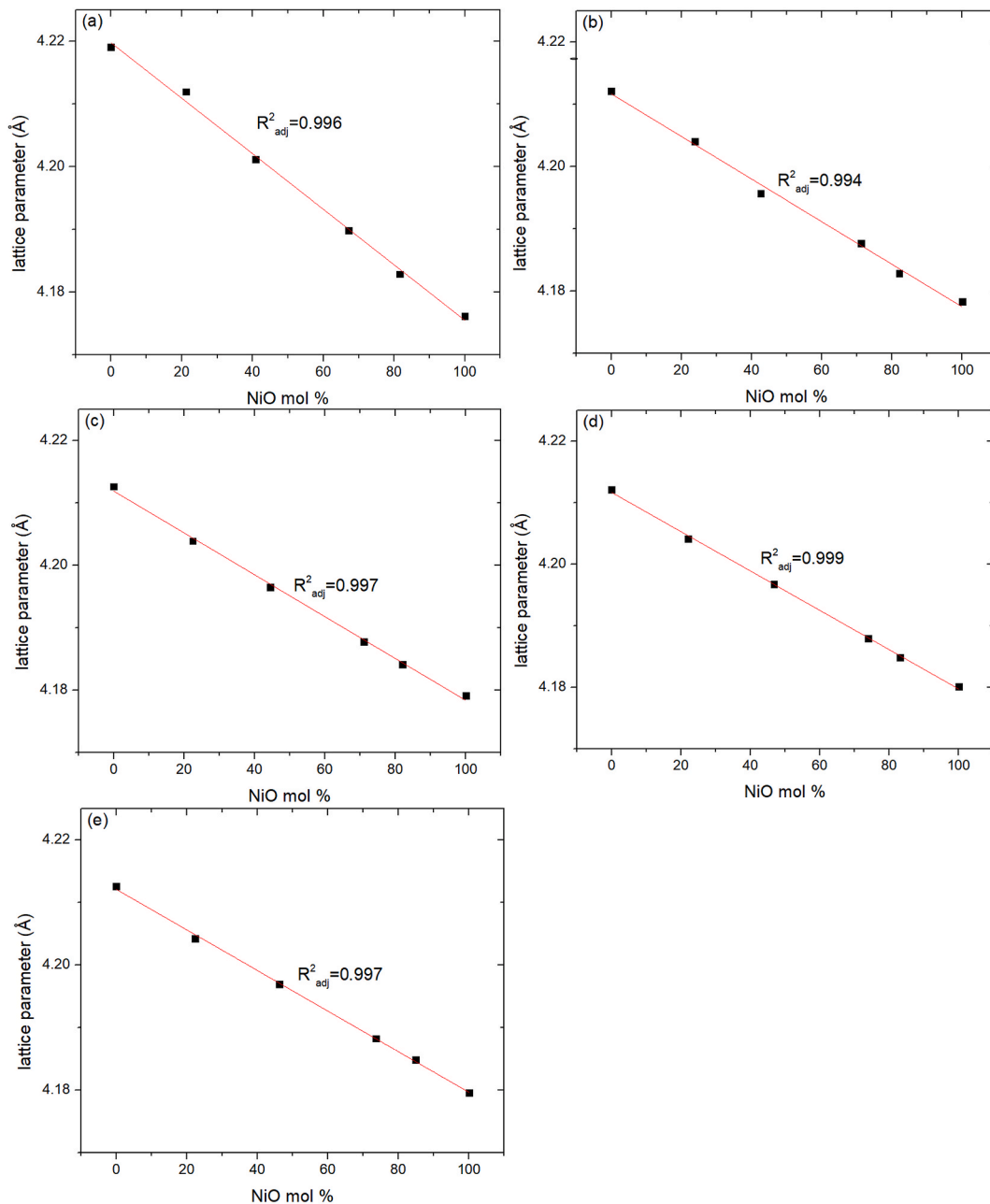
Fig. 7. Unit cell parameter versus concentration for samples calcined at temperatures 673, 873, 1073, 1273 and 1473 K signed as a,b,c,d and e respectively.

3.4. Unit cell parameter as a function of composition

The obtained results were also cross-checked by plotting the refined lattice unit cell parameters versus the refined composition yielding linear curves confirming Vegard's law (see Fig. 7). Vegard's law states that the lattice parameter of a solid solution of two constituents is approximately a weighted mean of the two constituents' lattice parameters at the same temperature. This comparison is suitable since cell parameters and intensities are independent variables in Rietveld refinement method. According to Fig. 7 as the concentration of MgO increased in the solid solution, the lattice parameter approached the lattice parameter of pure MgO. Conversely, with an increase in NiO concentration, the lattice parameter approached the lattice parameter of pure NiO. This behaviour is in accordance with Vegard's law. In addition, it was expected that as observed in Fig. 6 lattice variations versus grain size will affect the function of unit cell parameter versus concentration, becoming non-linear. However, it did not occur. This can be explained by the fact that grain size was generally similar at each temperature for all concentrations (See Table 2).

Table 2
Average grain size values of $Mg_{1-x}Ni_xO$ samples calcined at different calcination temperatures (the error is estimated as 10 %).

temperature (K)											
Sample ID Nominal % MgO	473	573	673	773	873	973	1073	1173	1273	1373	1473
0 [a]	c	8	20	30	52	c	200	c	350	c	453
0 [b]	3	8	17	30	38	51	57	67	75	90	120
20	c	6	10	c	36	c	175	c	300	c	461
40	c	5	9	c	44	c	187	c	300	c	446
60	c	5	8	c	36	c	173	c	240	c	289
80	c	4	6	c	28	c	123	c	219	c	310
100 [a]	c	25	27	c	106	c	119	c	170	c	255
100 [b]	c	28	29	35	36	36	48	56	53	77	114

[a] Gradual heating process.
[b] Direct heating process.
[c] Not measured.

Table 3
Representative micro-strain values $(X10^3)$ of $Mg_{1-x}Ni_xO$ samples calcined at different calcination temperatures (gradual heating process).

temperature (K)					
Sample ID Nominal % MgO e	673	873	1073	1273	1473
0	1.2	0.45	0.46	0.73	0.92
20	1.8	0.63	0.22	0.31	0.55
40	2.3	0.58	0.18	0.20	0.32
60	2.1	0.10	0.52	0.19	0.15
80	2.3	1.5	0.80	0.28	0.17
100	0.75	0.72	0.15	0.17	0.08

3.5. Grain size analysis and residual micro-strain

Micro-strain reflects the deviations in the peak positions due to non-uniform interplaner spacing. Micro-strain may exist in a single grain or reflect changes between grains. In the present case, the micro-strains are significantly higher in samples calcined at the low temperatures as shown in Table 3. This can be explained by the high slope of the lattice parameter versus grain size for small grains below 60–80 nm (as shown in Figs. 4 and 5). In addition, according to Figs. 4 and 5, there is some diversity in grain size in all samples. However, only in the nano range (below 60–80 nm) this diversity is accompanied with a large deviation in the lattice parameters (see Fig. 6) causing a micro-strain-like effect.

3.6. Unit cell parameter as a function of grain size

The average grain size of each sample increased with the increase in the calcination temperature, as anticipated. There was an agreement between the grain size evaluation from the XRD line broadening analysis and SEM observations (see Figs. 4 and 5).

Since it is known that in nanocrystalline oxides there is a variation of the lattice parameters with grain size, the lattice parameter was plotted versus grain size. A non-monotonic variation of the lattice parameter versus grain size was found in all samples (Fig. 8).

The idea that the specific surface area (m^2/mole) is an independent variable controlling nanostructures was stated by Navrotzky [74]. It was shown that amorphous zirconia, anatase (titania, TiO_2) and gamma alumina (γ-Al_2O_3) transformed to monoclinic zirconia, rutile (titania) and alpha alumina respectively, when the specific surface area increased. Kimmel and Zabicky [75] suggested a modified free Gibbs energy (G) formula for a particle free energy:

$$G = E_b + E_s \bullet \Lambda + PV - TS. \tag{3}$$

where E_b and E_s are the bulk and surface energies respectively, Λ is the area per volume ratio of the particle, P is pressure, V is volume, T is temperature and S is entropy.

Turning to specific terms, Eq. 2 becomes:

$$g = e_b + e_s \bullet \Lambda + P\rho - Ts. \tag{4}$$

where g is the specific free energy, e_b and e_s are the specific bulk and surface energies respectively, ρ is the specific volume and s is specific entropy. In large particles (micrometric and above) Λ is very small and it is possible to neglect the second term. However, in nanometric particles (where Λ is very large), Λ becomes the most important thermodynamic variable. There are two phenomena which may be observed. The first, is the formation of special nanostructures and particle shapes with a geometry suitable for a low Λ (to
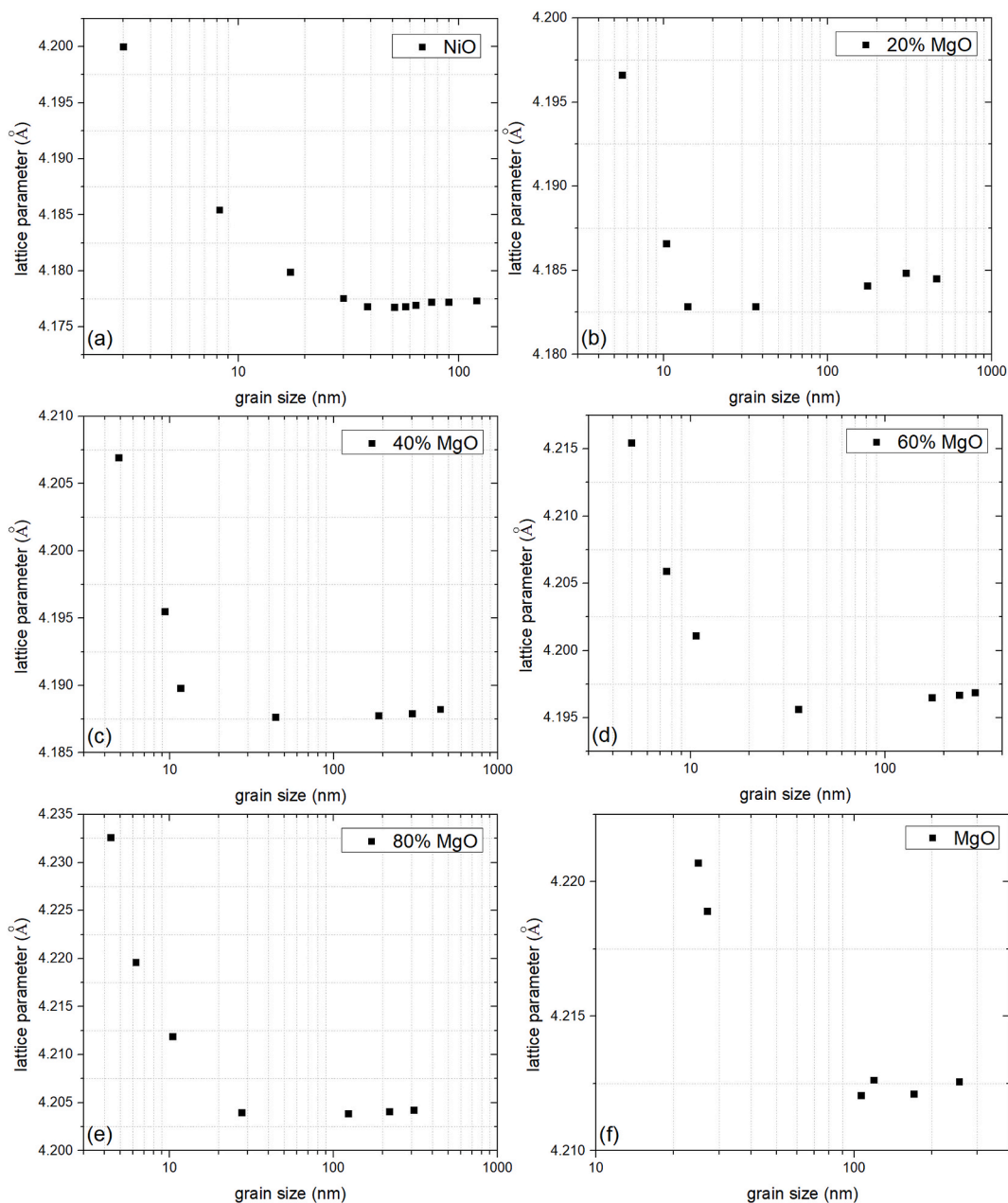
Fig. 8. The lattice parameter of $Mg_{1-x}Ni_xO$ as a function of the grain size in nm.

reduce the free energy). Therefore, nano crystals will grow as particles with the most symmetric structure, possible preferably cubic (a relatively low Λ). The second phenomenon is accompanied with the fact that Λ is a thermodynamic coordinate like P an T. Thus, all physical properties of a nanometric phase can vary as a function of Λ, analogous to their variation along P and T. Since $\Lambda \sim D^{-1}$, it was decided to add a presentation of the lattice parameters versus D^{-1} showing lattice expansion along increase of Λ.

A second order polynomial correlation between the unit cell lattices parameter and the inverse grain size was fitted for each concentration as shown by the equations in Fig. 9.

When grain size decreased, in the high nano range, there was a slight decrease of the lattice parameter. It might be attributed to the surface stress effect. In the low nano range, there was an expansion of the lattice parameter with the decreasing in grain size. It is understandable that this expansion is attributed to a weaker ionic bonding which is typical in nano grains. Due to a faster growth of pure MgO at low calcination temperatures in comparison to the samples with NiO, the effect of lattice expansion was minor in pure MgO causing shifting from the linear line of all other Mg:Ni ratios in samples calcined at temperatures of 573 and 673 K.
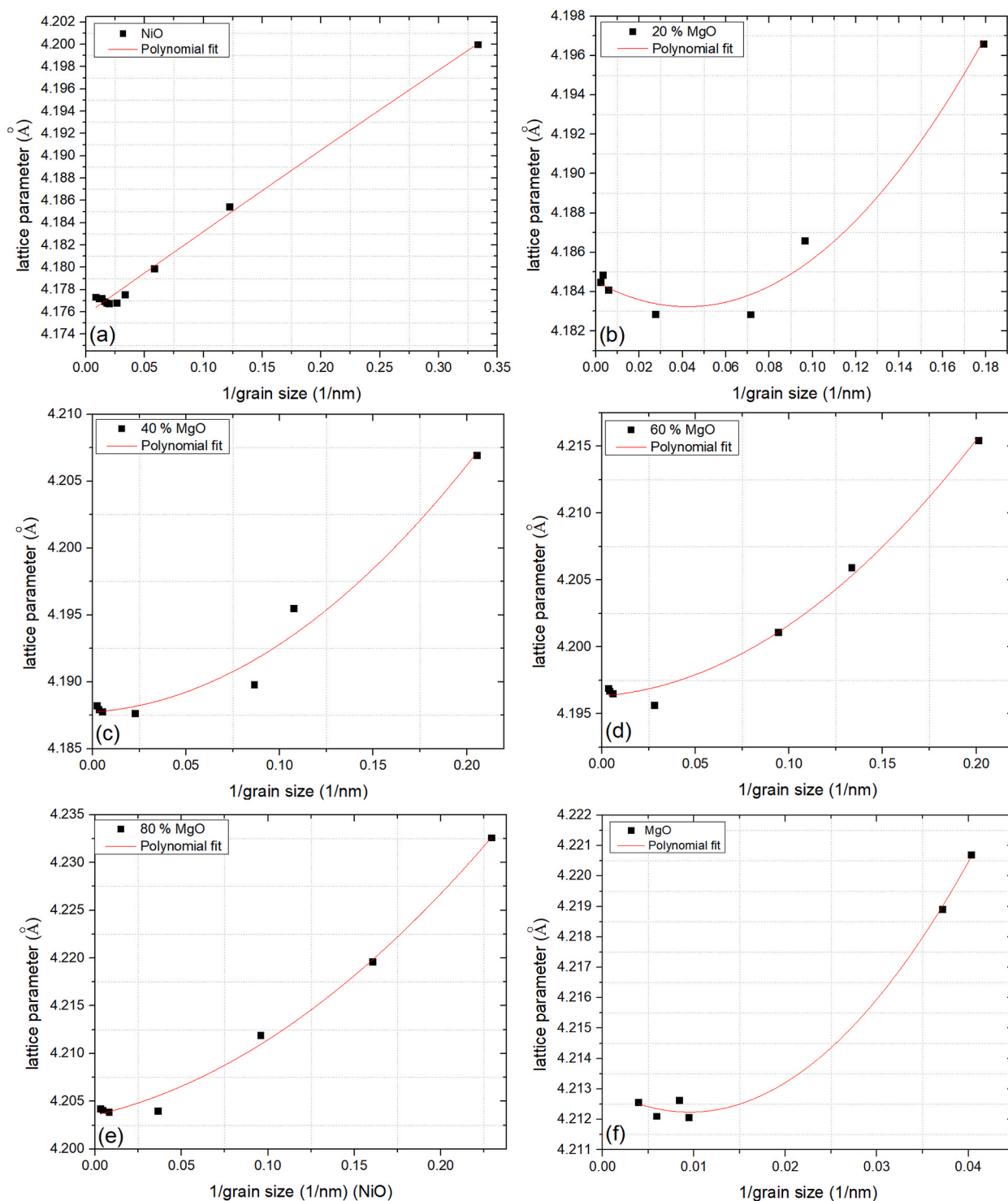
Fig. 9. The lattice parameter of $Mg_{1-x}Ni_xO$ as a function of the reversed grain size with a polynomial fit (second order).

3.7. The influence of preparation method on the lattice parameter

Since two sets of pure NiO and MgO powder samples were produced using two methods, a comparison of the behavior of the unit cell lattice parameter as a function of grain size was conceivable. The two powder sets of pure NiO and MgO were produced by two different comparable wet-chemistry synthesis routes: the microwave solvothermal method (as discussed previously in this study) and
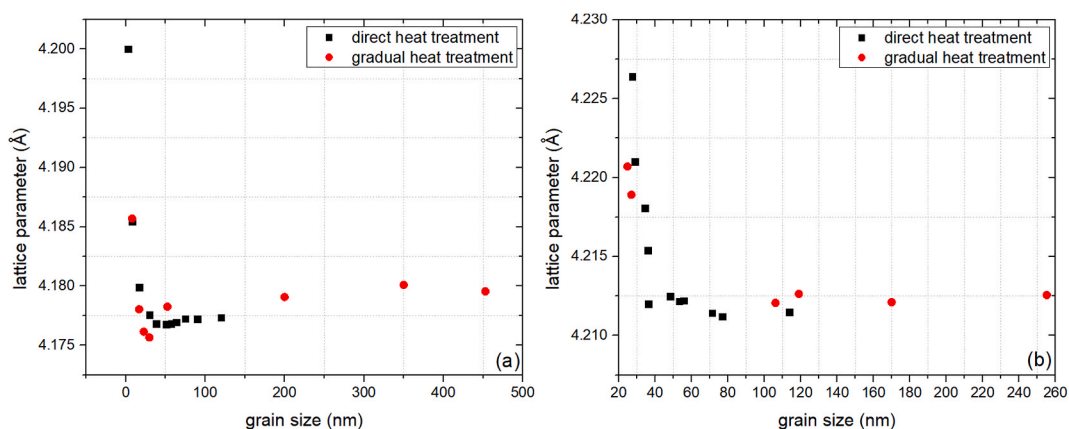
Fig. 10. The lattice parameter as a function of grain size in two different synthesis and heat treatments: (1) solvothermal microwave method followed by a gradual heat treatment and (2) sol-gel method followed by a direct heating treatment for (a) NiO and (b) MgO.

the sol-gel technique. In addition, the obtained preliminary powders were heat treated differently by: 1) a gradual heating treatment process following the microwave solvothermal method from room temperature to the desired final temperature and heating at a constant temperature for 30 min and through 2) a direct heating process following the sol-gel synthesis in which powders were inserted directly into a hot furnace at the desired annealing temperature for 3 h. The unit cell lattice parameter versus grain size is shown in Fig. 10 for: (a) two sets of NiO samples and (b) two sets of MgO samples.

It is also worth mentioning that nevertheless the XRD measurements were executed by two different diffractometers and by two different preparation methods followed by a different annealing process the curves displaying the variation of the lattice parameters versus grain size in Fig. 10 converged and complemented each other's trend regardless of the preparative procedure. In other words, the meaning is that the lattice parameter values are a function of grain size and are path independent.

4. Conclusions

The uniqueness of this research study is that a two-dimensional map of lattice parameter as a function of both grain size and composition of $Mg_{1-x}Ni_xO$ (for x values between 0.00 and 1.00) was obtained. Hence, the solid solution was obtained in several compositions and in a wide range of grain size and the aforementioned relation was found for all the compositions.

It is seen that the surface/volume (as well as specific surface area in units of m^2/mole) is an independent thermodynamic variable like temperature, pressure and concentration. In the presented experiments, each phase parameter may be continuously changed along the a above four thermodynamic coordinates. The lattice parameter was the investigated parameter. Since measurements were executed at ambient conditions the parameters of temperature and pressure were constant. However, two other thermodynamic coordinates remained. The traditional x (composition) and the novel parameter volume/surface $\Lambda \sim D^{-1}$ (D is the average grain size) served as a thermodynamic coordinate.

The present study confirmed the two stages of lattice parameter dependence - lattice contraction and lattice expansion are existing with decreasing the grain size nanoscale crystals, with a minimum lattice parameter for intermediate nano sizes, and a further increase for smaller sizes. According to this study and our previous studies [42,76], the non-monotonic lattice variation in nano-crystalline ionic materials is the general case. The non-monotonic lattice variation in nanomaterials calls for adding a new category in the crystallographic data bases: "nano-crystals", where lattice parameters are recorded along with grain size.

These findings can be significant for tailoring the properties and performance of materials based on the MgO–NiO system, particularly in applications where lattice matching and crystal structure control are crucial.

Data availability

Data will be made available on reasonable request.

Additional information

No additional information is available for this paper.

CRediT authorship contribution statement

Chen Barad: Writing – review & editing, Writing – original draft, Investigation. **Giora Kimmel:** Supervision, Project administration, Methodology, Investigation, Funding acquisition, Conceptualization. **Agnieszka Opalińska:** Formal analysis, Data curation.

Stanislaw Gierlotka: Resources, Methodology, Investigation. **Witold Łojkowski:** Resources, Methodology, Investigation.

Declaration of competing interest

The authors declare that they have no known competing financial interests or personal relationships that could have appeared to influence the work reported in this paper.

References

[1] J.P. Saikia, S. Paul, B.K. Konwar, S.K. Samdarshi, Nickel oxide nanoparticles: a novel antioxidant, Colloids Surf. B Biointerfaces 78 (1) (2010) 146–148.
[2] C. Mochizuki, Y. Inomata, S. Yasumura, M. Lin, A. Taketoshi, T. Honma, et al., Defective NiO as a stabilizer for Au single-atom catalysts, ACS Catal. 12 (10) (2022) 6149–6158.
[3] X. Xia, L. Fu, Z. Luo, J. Zhu, W. Yang, D. Li, et al., Discharge behavior of NiO as thermal battery cathode at ultrahigh temperature, Electrochem. Commun. 134 (2022) 107185.
[4] I. Hotový, J. Huran, L. Spiess, R. Čapkovic, Š. Haščík, Preparation and characterization of NiO thin films for gas sensor applications, Vacuum 58 (2–3) (2000) 300–307.
[5] C. Li, P.G. Choi, K. Kim, Y. Masuda, High performance acetone gas sensor based on ultrathin porous NiO nanosheet, Sensor. Actuator. B Chem. 367 (2022) 132143.
[6] G. Wang, X. Lu, T. Zhai, Y. Ling, H. Wang, Y. Tong, et al., Free-standing nickel oxide nanoflake arrays: synthesis and application for highly sensitive non-enzymatic glucose sensors, Nanoscale 4 (10) (2012) 3123–3127.
[7] Y. Ichiyanagi, N. Wakabayashi, J. Yamazaki, S. Yamada, Y. Kimishima, E. Komatsu, et al., Magnetic properties of NiO nanoparticles, Phys. B Condens. Matter 329 (2003) 862–863.
[8] X. Deng, Z. Chen, Preparation of nano-NiO by ammonia precipitation and reaction in solution and competitive balance, Mater. Lett. 58 (3–4) (2004) 276–280.
[9] H. Wang, Y. Lin, J. Lu, Ultra-thin nickel oxide overcoating of noble metal catalysts for directing selective hydrogenation of nitriles to secondary amines, Catal. Today 410 (2023) 253–263.
[10] S. Adhikari, A. Sarkar, B.B. Dhar, C–H bond chlorination using nickel (ii) complexes of tetradentate amido-quinoline ligands, Chem. Commun. 58 (25) (2022) 4075–4078.
[11] M.E. Begum, M.B. Islam, M.H. Ara, A. Doris, M.A. Kaiyum, M. Rasadujjaman, The prospect of spray pyrolyzed pure, Mn-doped, and Zn-doped nickel oxide thin films as TCO material, Heliyon 10 (1) (2024) e24244.
[12] S. Abinaya, H.P. Kavitha, M. Prakash, A. Muthukrishnaraj, Green synthesis of magnesium oxide nanoparticles and its applications: a review, Sustainable Chemistry and Pharmacy 19 (2021) 100368.
[13] J.P. Singh, V. Singh, A. Sharma, G. Pandey, K.H. Chae, S. Lee, Approaches to synthesize MgO nanostructures for diverse applications, Heliyon 6 (9) (2020) e04882.
[14] M. Fernandes, K. Rb Singh, T. Sarkar, P. Singh, R. Pratap Singh, Recent applications of magnesium oxide (MgO) nanoparticles in various domains, Adv. Mater. Lett. 11 (8) (2020) 1–10.
[15] W. Yang, J.I. Peters, I.I.I.R.O. Williams, Inhaled nanoparticles—a current review, Int. J. Pharm. 356 (1–2) (2008) 239–247.
[16] C. Buzea, I.I. Pacheco, K. Robbie, Nanomaterials and nanoparticles: sources and toxicity, Biointerphases 2 (4) (2007) MR17–71.
[17] M.M. Imani, M. Safaei, Optimized synthesis of magnesium oxide nanoparticles as bactericidal agents, Journal of Nanotechnology 2019 (2019).
[18] Z. Tang, B. Lv, MgO nanoparticles as antibacterial agent: preparation and activity, Braz. J. Chem. Eng. 31 (2014) 591–601.
[19] K. Krishnamoorthy, J.Y. Moon, H.B. Hyun, S.K. Cho, S. Kim, Mechanistic investigation on the toxicity of MgO nanoparticles toward cancer cells, J. Mater. Chem. 22 (47) (2012) 24610–24617.
[20] Z. Camtakan, S. Erenturk, S. Yusan, Magnesium oxide nanoparticles: preparation, characterization, and uranium sorption properties, Environ. Prog. Sustain. Energy 31 (4) (2012) 536–543.
[21] J.I. Di Cosimo, V.K. Díez, C. Ferretti, C.R. Apesteguía, Basic catalysis on MgO: generation, characterization and catalytic properties of active sites, Catalysis 26 (3000) (2014) 1–28.
[22] Z. Taherian, A. Khataee, Y. Orooji, Facile synthesis of yttria-promoted nickel catalysts supported on MgO-MCM-41 for syngas production from greenhouse gases, Renew. Sustain. Energy Rev. 134 (2020) 110130.
[23] V. Gulino, M. Brighi, F. Murgia, P. Ngene, P. De Jongh, R. Černý, et al., Room-temperature solid-state lithium-ion battery using a LiBH4–MgO composite electrolyte, ACS Appl. Energy Mater. 4 (2) (2021) 1228–1236.
[24] B. Xiao, P. Wang, Z. He, Z. Yang, L. Tang, C. An, et al., Effect of MgO and TiO2 coating on the electrochemical performance of Li-rich cathode materials for lithium-ion batteries, Energy Technol. 7 (8) (2019) 1800829.
[25] M. Rashad, Performance efficiency and kinetic studies of water purification using ZnO and MgO nanoparticles for potassium permanganate, Opt. Quant. Electron. 51 (2019) 1–13.
[26] Y. Haldorai, J. Shim, An efficient removal of methyl orange dye from aqueous solution by adsorption onto chitosan/MgO composite: a novel reusable adsorbent, Appl. Surf. Sci. 292 (2014) 447–453.
[27] W.A. Khaleel, S.A. Sadeq, I.A.M. Alani, M.H.M. Ahmed, Magnesium oxide (MgO) thin film as saturable absorber for passively mode locked erbium-doped fiber laser, Opt Laser. Technol. 115 (2019) 331–336.
[28] I.V. Kozerozhets, G.P. Panasyuk, L.A. Azarova, V.N. Belan, E.A. Semenov, I.L. Voroshilov, et al., Acquisition, properties, and application of nanosized magnesium oxide powders: an overview, Theor. Found. Chem. Eng. 55 (2021) 1126–1132.
[29] A.M. Abyzov, Research on the development of high-quality aluminum oxide ceramic (review). Part 1. Sintering with additives, reactive sintering, production of reinforced composites, Glass Ceram. 75 (2018) 293–302.
[30] H. Li, Q. Tian, H. Zhao, A. Lu, J. Liu, Temperature sensitivity of MgO expansive agent and its application in temperature crack mitigation in shiplock mass concrete, Construct. Build. Mater. 170 (2018) 613–618.
[31] N.M. Rasi, A. Karcz, S. Ponnurangam, N. Mahinpey, Insight into MgO-supported NiO reactivity from atomic-scale electronegativity for oxygen carrier design and catalyst production applications, Catal. Today 404 (2022) 244–252.
[32] A. Ghaemi, H. Mashhadimoslem, P. Zohourian Izadpanah, NiO and MgO/activated carbon as an efficient CO2 adsorbent: characterization, modeling, and optimization, Int. J. Environ. Sci. Technol. 19 (2) (2022) 727–746.
[33] J. Wang, Z. Huang, Y. Wang, J. Wu, Z. Rao, F. Wang, et al., Low temperature conversion of methane to syngas using lattice oxygen over NiO-MgO, Chin. Chem. Lett. 33 (10) (2022) 4687–4690.
[34] M. Chuenjai, S. Wongsakulphasatch, N. Yong, W. Maneeprakorn, K. Sudsakorn, V. Tongnan, et al., Synthesis of NiO/MgO/ZrO2 catalyst for syngas production from partial oxidation and dry reforming of biogas, Int. J. Hydrogen Energy 47 (98) (2022) 41386–41396.
[35] A. Kerrigan, K. Pande, D. Pingstone, S.A. Cavill, M. Gajdardziska-Josifovska, K.P. McKenna, et al., Nano-faceted stabilization of polar-oxide thin films: the case of MgO (111) and NiO (111) surfaces, Appl. Surf. Sci. 596 (2022) 153490.
[36] W. Fu, J. Pan, J. Niu, Y. Fu, G. Xiao, J. Wang, et al., A transparent photovoltaic device of NiO/MgO quantum dots/TiO2 arrays pn junction with carrier injection of MgO QDs, J. Mater. Sci. Mater. Electron. 33 (2) (2022) 652–662.
[37] M. Serra, P. Salagre, Y. Cesteros, F. Medina, J.E. Sueiras, Study of preparation conditions of NiO–MgO systems to control the morphology and particle size of the NiO phase, Solid State Ionics 134 (3–4) (2000) 229–239.

[38] T.B. Rymer, The lattice constants of small crystals, Il Nuovo Cimento Series 10 (6) (1957) 294–305.

[39] P.M. Diehm, P. Ágoston, K. Albe, Size-dependent lattice expansion in nanoparticles: reality or anomaly? ChemPhysChem 13 (10) (2012) 2443–2454.

[40] H. Zhang, B. Chen, J.F. Banfield, The size dependence of the surface free energy of titania nanocrystals, Phys. Chem. Chem. Phys. 11 (14) (2009) 2553–2558.

[41] Q. Jiang, L.H. Liang, D.S. Zhao, Lattice contraction and surface stress of fcc nanocrystals, J. Phys. Chem. B 105 (27) (2001) 6275–6277.

[42] G. Kimmel, A. Sahartov, Y. Sadia, Z. Porat, J. Zabicky, E. Dvir, Non-monotonic lattice parameters variation with crystal size in nanocrystalline CeO2, J. Mater. Res. Technol. 12 (2021) 87–99.

[43] G.K. Rane, U. Welzel, S.R. Meka, E.J. Mittemeijer, Non-monotonic lattice parameter variation with crystallite size in nanocrystalline solids, Acta Mater. 61 (12) (2013) 4524–4533.

[44] A.K. Srivastav, N. Chawake, B.S. Murty, Grain-size-dependent non-monotonic lattice parameter variation in nanocrystalline W: the role of non-equilibrium grain boundary structure, Scripta Mater. 98 (2015) 20–23.

[45] W.H. Qi, M.P. Wang, Size effect on the cohesive energy of nanoparticle, J. Mater. Sci. Lett. 21 (2002) 1743–1745.

[46] Y.F. Zhu, W.T. Zheng, Q. Jiang, Modeling lattice expansion and cohesive energy of nanostructured materials, Appl. Phys. Lett. 95 (8) (2009).

[47] D.K.C. Macdonald, K. Sarginson, Size effect variation of the electrical conductivity of metals, Proc. Roy. Soc. Lond. Math. Phys. Sci. 203 (1073) (1950) 223–240.

[48] S.M. Rossnagel, T. Kuan, Alteration of Cu conductivity in the size effect regime, J. Vac. Sci. Technol. B: Microelectronics and Nanometer Structures Processing, Measurement, and Phenomena 22 (1) (2004) 240–247.

[49] B. Feng, Z. Li, X. Zhang, Prediction of size effect on thermal conductivity of nanoscale metallic films, Thin Solid Films 517 (8) (2009) 2803–2807.

[50] P. Villain, P. Goudeau, P. Renault, K.F. Badawi, Size effect on intragranular elastic constants in thin tungsten films, Appl. Phys. Lett. 81 (23) (2002) 4365–4367.

[51] A.C. Bose, P. Balaya, P. Thangadurai, S. Ramasamy, Grain size effect on the universality of AC conductivity in SnO2, J. Phys. Chem. Solid. 64 (4) (2003) 659–663.

[52] D. McCauley, R.E. Newnham, C.A. Randall, Intrinsic size effects in a barium titanate glass-ceramic, J. Am. Ceram. Soc. 81 (4) (1998) 979–987.

[53] Z. Xu, F. Xiao, S.K. Purnell, O. Alexeev, S. Kawi, S.E. Deutsch, et al., Size-dependent catalytic activity of supported metal clusters, Nature 372 (6504) (1994) 346–348.

[54] S. Zhou, L. He, S. Zhao, Y. Guo, J. Zhao, L. Shi, Size-dependent structural and magnetic properties of LaCoO3 nanoparticles, J. Phys. Chem. C 113 (31) (2009) 13522–13526.

[55] P.P. Rodenbough, C. Zheng, Y. Liu, C. Hui, Y. Xia, Z. Ran, et al., Lattice expansion in metal oxide nanoparticles: MgO, Co3O4, & Fe3O4, J. Am. Ceram. Soc. 100 (1) (2017) 384–392.

[56] T. Van Buuren, L.N. Dinh, L.L. Chase, W.J. Siekhaus, L.J. Terminello, Changes in the electronic properties of Si nanocrystals as a function of particle size, Phys. Rev. Lett. 80 (17) (1998) 3803.

[57] C.I. Zandalazini, J.N. Sanchez, E.A. Albanesi, Y. Gupta, P. Arun, Contribution of lattice parameter and vacancies on anisotropic optical properties of tin sulphide, J. Alloys Compd. 746 (2018) 9–18.

[58] V. Perebeinos, S. Chan, F. Zhang, 'Madelung model'prediction for dependence of lattice parameter on nanocrystal size, Solid State Commun. 123 (6–7) (2002) 295–297.

[59] S. Maitra, J. Roy, Nanoceramic matrix composites: types, processing, and applications. Advances in Ceramic Matrix Composites, 2018, pp. 27–48.

[60] R.A. McINTYRE, Common nano-materials and their use in real world applications, Sci. Prog. 95 (1) (2012) 1–22.

[61] A. Nouri, A. Sola, Powder morphology in thermal spraying, J. Adv. Manuf. Process. 1 (3) (2019) e10020.

[62] T.M. Crowder, J.A. Rosati, J.D. Schroeter, A.J. Hickey, T.B. Martonen, Fundamental effects of particle morphology on lung delivery: predictions of Stokes' law and the particular relevance to dry powder inhaler formulation and development, Pharm. Res. (N. Y.) 19 (2002) 239–245.

[63] H. Shimada, Morphology and orientation of MoS2 clusters on Al2O3 and TiO2 supports and their effect on catalytic performance, Catal. Today 86 (1–4) (2003) 17–29.

[64] Z. Qiao, Z. Wu, S. Dai, Shape-controlled ceria-based nanostructures for catalysis applications, ChemSusChem 6 (10) (2013) 1821–1833.

[65] B. Rebours, J. d'Espinose de la Caillerie, O. Clause, Decoration of nickel and magnesium oxide crystallites with spinel-type phases, J. Am. Chem. Soc. 116 (5) (1994) 1707–1717.

[66] L. Chen, X. Sun, Y. Liu, Y. Li, Preparation and characterization of porous MgO and NiO/MgO nanocomposites, Appl. Catal. Gen. 265 (1) (2004) 123–128.

[67] A. Janotti, D. Segev, C.G. Van de Walle, Effects of cation d states on the structural and electronic properties of III-nitride and II-oxide wide-band-gap semiconductors, Phys. Rev. B 74 (4) (2006) 045202.

[68] S. Valanarasu, V. Dhanasekaran, M. Karunakaran, T.A. Vijayan, R. Chandramohan, T. Mahalingam, Microstructural, optical and electrical properties of various time annealed spin coated MgO thin films, J. Mater. Sci. Mater. Electron. 25 (2014) 3846–3853.

[69] Y.G. Zhang, H.Y. He, B.C. Pan, Structural features and electronic properties of MgO nanosheets and nanobelts, J. Phys. Chem. C 116 (43) (2012) 23130–23135.

[70] R.A. Young, D.B. Wiles, Application of the Rietveld method for structure refinement with powder diffraction data, Adv. X Ray Anal. 24 (1980) 1–23.

[71] Rodrigez-Carvajal, Fullprof, Program for Rietveld Refinment, 3.7, 1997.

[72] T. Roisnel, J. Rodríguez-Carvajal, J. Gonzalez-Platas, WinPLOTR, a Graphic Tool for Powder Diffraction, Laboratoire Léon Brillouin (CEA/CNRS), CEA-Saclay, 2001 91191.

[73] W. Kraus, G. Nolze, POWDER CELL–a program for the representation and manipulation of crystal structures and calculation of the resulting X-ray powder patterns, J. Appl. Crystallogr. 29 (3) (1996) 301–303.

[74] A. Navrotsky, Energetics of nanoparticle oxides: interplay between surface energy and polymorphism, Geochem. Trans. 4 (2003) 1–4.

[75] G. Kimmel, J. Zabicky, Stability, instability, metastability and grain size in nanocrystalline ceramic oxide systems, Solid State Phenom. 140 (2008) 29–36.

[76] C. Barad, G. Kimmel, B.A. Rosen, A. Sahartov, H. Hayun, J. Zabicky, et al., Lattice variation of cubic Y2O3 in three dimensions: temperature, pressure and crystal size, J. Alloys Compd. 885 (2021) 161199.